Contents list available at IJRED website

Int. Journal of Renewable Energy Development (IJRED)

Journal homepage: http://ejournal.undip.ac.id/index.php/ijred

Research Article

CFD Investigation of A New Elliptical-Bladed Multistage Savonius Rotors

Khalid Mrigua*[a], Abdelghani Toumi[b], Mounia Zemamou[a], Bader Ouhmmou[a] , Yahya Lahlou[a], Mohammed Aggour[a].

[a]*Laboratory of Renewable Energy, Faculty of Science, Ibn Tofail University, Kenitra, Morocco*

[b]*Laboratoire D'ingénierie, Management Industriel et Innovation Université Hassan, Settat, Morocco.*

ABSTRACT. The Savonius-conventional wind turbine is a class of wind turbines designed with a vertical axis. It has a good starting capacity and an insensitivity to wind direction. It works relatively at low wind speed in an easy installation. Savonius wind turbine faces major drawbacks, including some of the low efficiency and high negative torque created by the returning blade. Many attempts have been undertaken to optimize the blade's shape to increase the performance of these wind turbines. The vertical axis is still under development. The elliptical-blades with a cut angle equal 47.50° have recently shown enhanced performance. In this study, we investigate the effect of Elliptical-bladed multistage Savonius Rotors (rotor aspect ratio, stage aspect ratio) on the performance by means of numerical simulation. The results obtained by comparison of one, two, and three-stage rotors indicate that the maximum power coefficient increase with a number of the stages (for the rotors with similar RAR of 0.7). Moreover, for the rotors with similar SAR of 0.7, the two stages have the highest performance than others. ©2020. CBIORE-IJRED. All rights reserved

Keywords: Savonius rotor, Wind energy, multistage, numerical simulation

Article History: Received:17th April 2020; Revised: 25th June 2020; Accepted: 29th June 2020; Available online: 1st July 2020
How to Cite This Article: Mrigua, K., Toumi, A., Zemamou, M., Ouhmmou, B., Lahlou, Y., Aggour, M. (2020) CFD Investigation of a New Elliptical-Bladed Multistage Savonius Rotors. *International Journal of Renewable Energy Development*, 9(3), 383-392.
https://doi.org/10.14710/ijred.2020.30286

1. Introduction

Wind energy is an inexhaustible source of energy and dependent on the wind. It is, therefore, a real renewable resource that does not cause pollution, no CO_2 emission, and no toxic or dangerous substances freed into the environment. As wind energy depends on the cubic speed of the wind, a small increase in this parameter will increase the output power of the turbine. Furthermore, depending on the position of the rotor axis relative to the wind, wind turbines are generally classified into two types: wind turbines with the horizontal hub (HAWT) and wind turbines with the vertical hub (VAWT). The VAWTs are classified into two principal families: Darrieus-type (D-VAWT) and Savonius-type(S-VAWT). The most notable difference between the two is that the (D-VAWT) is named a lift turbine and the (S-VAWT) is named a drag turbine (ElCheikh *et al.* 2018). Savonius-type was developed by Sigurd Savonius, in 1925 (Ushiyama & Nagai. 1988).

The shape of the Savonius blade profile affects the rotor's performance significantly, in this context several studies attempt to enhance efficiency of conventional savonius turbines. Figure 1 illustrates different improved blade designs mainly, Elliptical blade tested by (Banerjee *et al.* 2014; Zemamou *et al.* 2019; Alom and Saha. 2019), Fig-1(b). Other researchers have investigated the performance of the savonius rotor formed of a straight segment and two arcs knowns as Benesh model (Roy & Saha. 2015; Benesh. 1988), and (Scheaua, 2020) Fig-1(c). In the same perspective, Bach model has been developed by (Roy & Saha. 2015; Kacprzak *et al.* 2013) and (Kamoji *et al.* 2009) in Fig-1(d). In order to reduce the negative torque exerted on the returning blade, Nugroho *et al.* (2020) have developed a Slotted-blade as depicted in Fig.1(e). Zemamou *et al.* (2020) have introduced a novel blade design based on polynomial Bezier curves Fig.1(f).

Twisted blade have been developed by (Grinspan *et al.* 2001; Saha et al. 2008; and Mendoza et al. 2020), as shown in Fig-1(g). Saha & Rajkumar (2006) have compared the performances of the Savonius rotor by varying the torsion angles. The results presented that the C_P of the twisted blades of a rotor could be changed by varying the twisted angle. The value of the optimal torsion angle is 15°, corresponding to maximum $C_p = 0.14$.

* Corresponding author: khalid.mrigua@uit.ac.ma

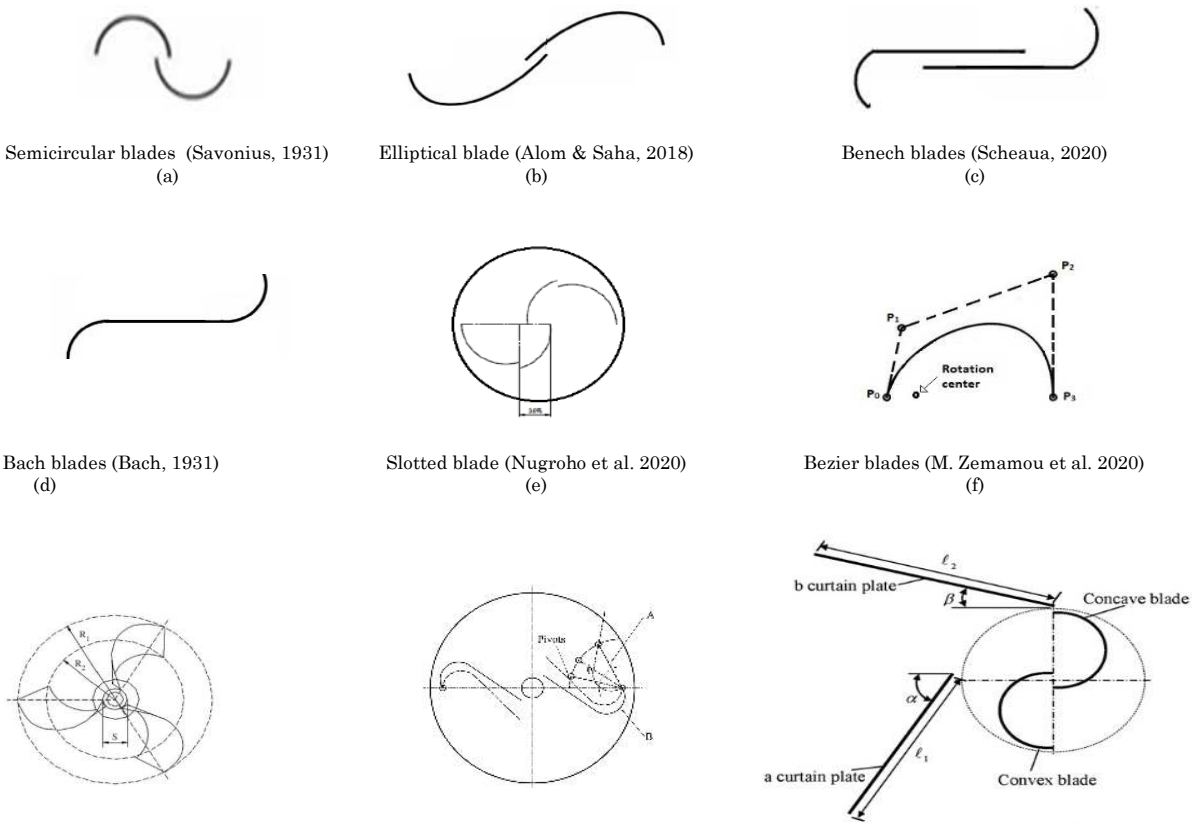

Semicircular blades (Savonius, 1931) (a) | Elliptical blade (Alom & Saha, 2018) (b) | Benech blades (Scheaua, 2020) (c)

Bach blades (Bach, 1931) (d) | Slotted blade (Nugroho et al. 2020) (e) | Bezier blades (M. Zemamou et al. 2020) (f)

Twisted blades (Saha & Rajkumar, 2006)) (g) | Swinging blades (Aldos, 1984) (h) | Curtain arrangement (Altan, & Atılgan,2010) (i)

Fig .1 Various types of blades used for Savonius

The performance coefficient of an (S-VAWT) is influenced by different parameters like overlap ratio OR, aspect ratio (AR), number of blades, shape of the blades and number of stages. Many researchers have carried out divers numerical and experimental researchers to improve the performance of an (S-VAWT), the overlap ratio of the Savonius turbines has a significant impact in the amelioration of the performance of these turbines, it is defined by the following equation (e/d) where (d) is the blade chord length and (e) represents the overlap.

In an experimental investigation, (Mojola, 1985) studied the effect of OR on the rotor performance, it is found that the maximum power of coefficient corresponds to an overlap ratio of about 0.25. According to (Akwa *et al.* 2012) the optimal value for the overlap ratio is 0.15. The latter corresponds to an average power coefficient equal to 0.3161. From a numerical investigation, (Alom & Saha, 2017) also produced that the overlap ratio value of 0.15 gives a higher performance.

An experimental analysis has been conducted by (Roy & Saha. 2013a) based on the variation of the aspect ratio. Results have shown that the rotor with the aspect ratio equal to 0.8 gives a higher coefficient of power C_{pmax}=0.178. Kamoji *et al.* (2009) concluded experimentally that the power and torque coefficients are maximum for an aspect ratio of 0.7.

The effect on a number of the blade has been investigated by (Blackwell *et al.* 1977), they found that two-blade Savonius turbines have a better power coefficient when compared with three-blade Savonius, (Mahmoud *et al.* 2012) , also noticed that the two-blade gave a better power coefficient than three and four ones. Indeed, the addition of blades disturbs the flow near the returning blade.

The use of multi-staging reduces the high fluctuation of torque without significant performance loss of the turbine, operating with cycles lagged relatively to one another. In the experimental analysis Mahmoud *et al.* (2012) concluded that the two stages rotor have a higher specific power. Hayashi *et al.* (2005) found that the values of C_{Pmax} and C_{Tmax} of the rotor with one-stage were much higher than those of the three-stage rotor. Saha *et al.* (2008) asserted that the rotor with two-stage and two-blade has a better aerodynamic performance than the others. However, from this study, a C_{pmax} of 0.31 and 0.29 is reached for twisted and Semicircular geometry blade profile respectively. Frikha *et al.* (2016) studied the effect of the number of stages on performance. The results showed an improvement of the dynamic torque coefficient

and the power coefficient as a function of the number of stages, they found that the C_{pmax} = 0.132 for the five-stage rotor. Kamoji *et al.* (2008) found that by increasing Reynolds number the power and torque coefficients increase. However, the rotors with three and two stages are the same performance for the same SAR of 1. In an experimental investigation, Chen *et al.* (2016) found for two-stage that the azimuth angle range of negative C_{TS} decreases by increasing GR. According to Menet (2004), the rotor with two-stage has a superior power coefficient (C_p) over the one stage rotor.

To reduce the converse force on the returning blade (Golecha *et al.* 2011) proposed to use the deflecting plate in front of the returning blade. Their result showed in optimal position the power coefficient improved by 50%. In addition, Ogawa *et al.* (1989) attained a maximum power of 0.27 when the plate with A =0.5R and B = R is placed at θ= 30°. In the same perspective, (Altan & Atılgan. 2010) has investigated the effect of curtain arrangement on performance. They found that the greatest performance has been obtained from curtain l_1 = 0.34 m and l_2 = 0.39 m at its position θ=60° for the angles α =45°, β=15°, Fig-1(i).

It is during the last few years many studies have been carried out to demonstrate the influence of modified savonius design on the performance. The general objective of this study to optimize the different parameters of the modified multistage Savonius rotor (Table 1) to reach at an appropriate design configuration. Savonius modified wind rotor comprises two elliptical blades, placed between two end plates as illustrated in Fig. 2. Based on the work of a previous study (Alom *et al.* 2016) the value of the aspect ratio AR = (H/D) is chosen 0.7.

2. Methodology

The multistage savonius rotors with the elliptical blade are tested numerically at various stage number (SN). The 3D unsteady simulation is realized by using pressure-based finite volume method (FVM) solver ANSYS Fluent. The power and torque coefficients are evaluated with respect to TSR. The SN is varied from 1 to 3 as illustrated in Figures 3 and Figure 4.

The dimensions of the elliptical blade are dictated by the ratio OB/OP=2/3 (Figure 5), similar to that the overall diameter of the turbine is 0.514 m, whereas the blade thickness is taken as 0.0066 m. The ratio OM/OA is taken as 0.54, to determine the required blade chord length (d) (Fig 5). Recently, the elliptical blade with a cutting angle θ = 47.5° showed improved performance than the traditional savonius rotor (Alom *et al.* 2016). The value of overlap ratio is taken as 0.2 (Alom & Saha 2017). Fig 5 shows the two-dimensional view of the elliptical blade.

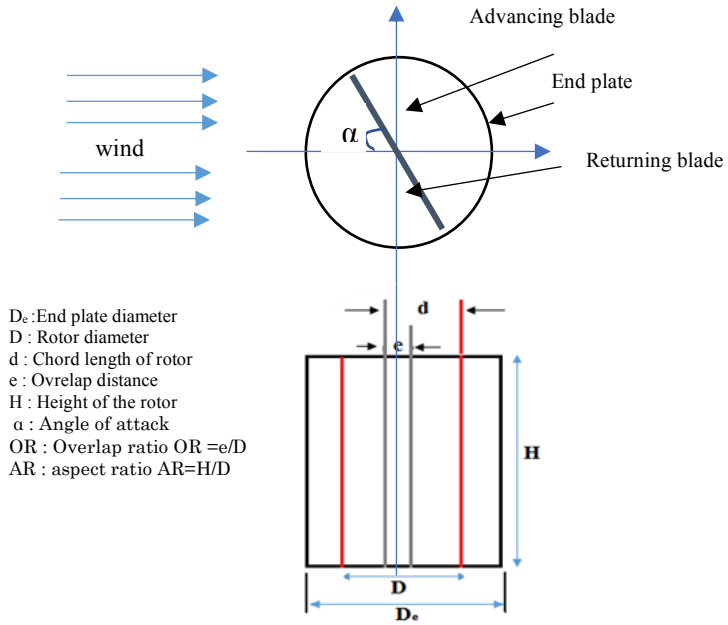

Fig. 2 A typical two elliptical blade Savonius rotor

Table 1
Geometrical parameters of elliptical Savonius rotors.

Geometrical parameters (m)				
Rotor diameter D	Rotor height H	End plate D_0	Chord of blade	Gap distance (e)
0.514	0.3598	0.5654	0.2855	0.0571

2.1 Mathematical formulation

The power of wind depends on the air density (ρ), the swept area (A), and the cubic wind speed (V^3) is given by (Roy & Saha. 2013b):

$$P_{available} = \frac{1}{2}\rho A V^3 \quad (1)$$

The coefficient of power (C_P) the rotor is defined from the relationship below (Roy & Saha. 2013b).

$$C_p = \frac{P_{turbine}}{P_{available}} = \frac{T \times \omega_s}{\frac{1}{2}\rho A V^3} = \frac{2\pi NT}{60 \times \frac{1}{2}\rho A V^3} \quad (2)$$

Where $P_{turbines:}$ power actually provided by the turbine. The relationship between the aerodynamic coefficients, is represented by the following equations.

$$C_p = \frac{P_{turbine}}{P_{available}} = \frac{T.\omega_s}{\frac{1}{2}\rho A V^3} = \frac{T \,.\, R\omega_s}{\frac{1}{2}\rho A V^2 R \quad V} \quad (3)$$

$$C_p = C_T \times TSR \quad (4)$$

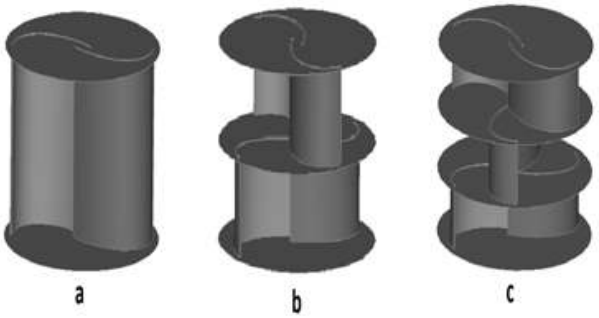

Fig. 3 Elliptical Savonius turbines with a RAR = 0.7 (a) Single-stage (b) Two-stage rotor (c) Three-stage

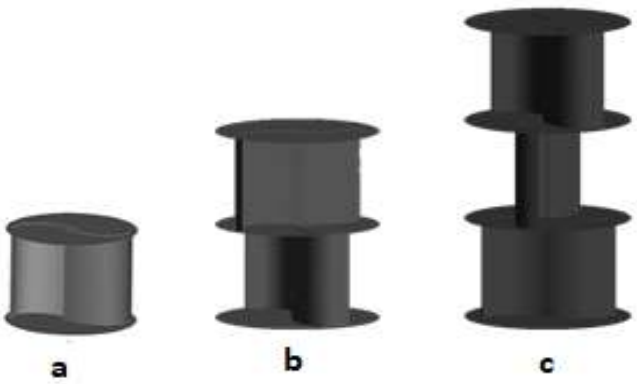

Fig. 4 Elliptical Savonius turbines with a SAR = 0.7 (a) Single-stage rotor with RAR = 0.7 (b) Two stages with RAR = 1.4 (c) Three stages with RAR = 2.1

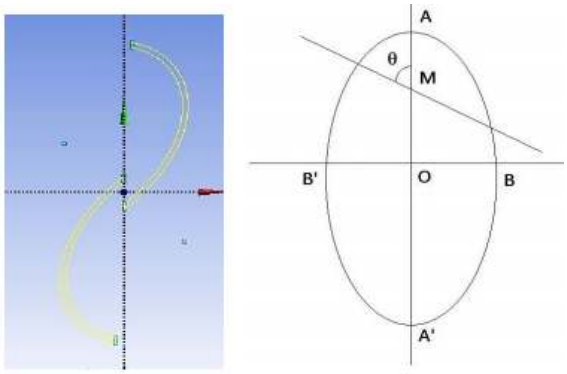

Fig 5. 2D view of a section cut on elliptical blade an ellipse (Alom *et al*. 2016)

2.2 Simulation domain and Boundary Condition

The three dimensions computational domain and Boundary condition for the Savonius rotor are shown in Figure 6. Indeed, the simulation domain has two subdomains separated by a sliding interface: a rotate and fluid domain. the dimension of the fluid domain is 10D × 5D × 4D. The Savonius rotors are located at the center of the rotate domain. The computational domain has been discretized by unstructured triangular grids mesh (Fig. 8). y^+ is an important parameter for calculating the value of the distance from the first node to the wall. The thickness of the first layer from the rotor surface is calculated using the following relation:

$$y^+ = \frac{\rho u_t y}{\mu} \quad (5)$$

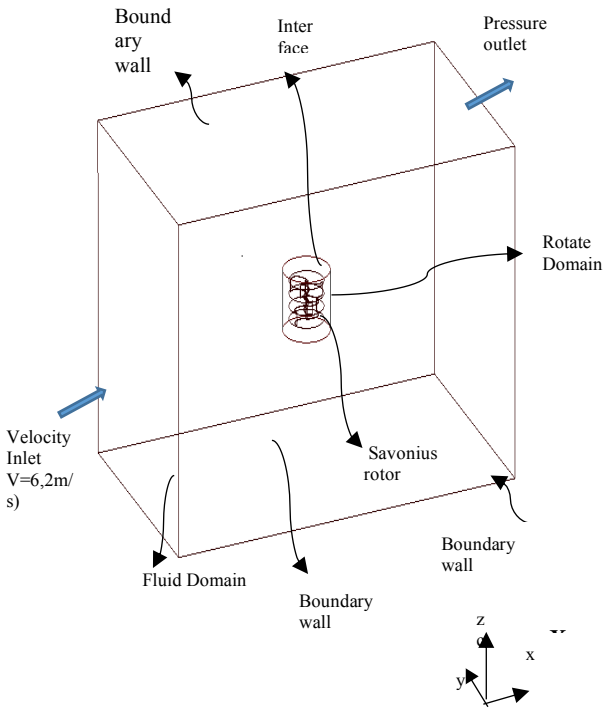

Fig. 6 Three-dimensional simulations domain

The frictional velocity is calculated from the following equation:

$$u_t = (\frac{\tau_\omega}{\rho})^{\frac{1}{2}} \quad (6)$$

Where τ_ω is wall shear stress, y distance of first cell from rotors wall and $\mu = 1.81 \cdot 10^5$ Ns.m^{-2} is the dynamic viscosity. In this work the first layer is set to be $5 \cdot 10^{-5}$ m and the growth rate of 1.2 (Fig. 8). For this study, we fix five complete rotations of the turbine. The maximum iteration by time step are 30. Absolute criteria are used to monitor the convergence of the solution with a value of 10^{-3}. The grid-independent test has been performed by varying the grids between 1147050 and 5826499 (Fig. 7). The simulation results show that there is no significant change in the coefficient of torque beyond 3439589 elements. The grid with 3439589 cells is adopted for all simulations.

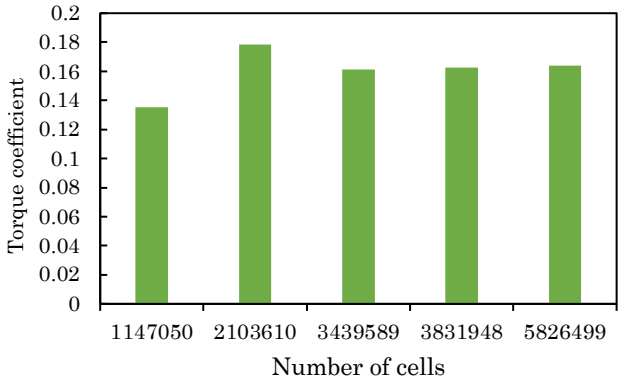

Fig. 7 Torque coefficient variation with number of cells

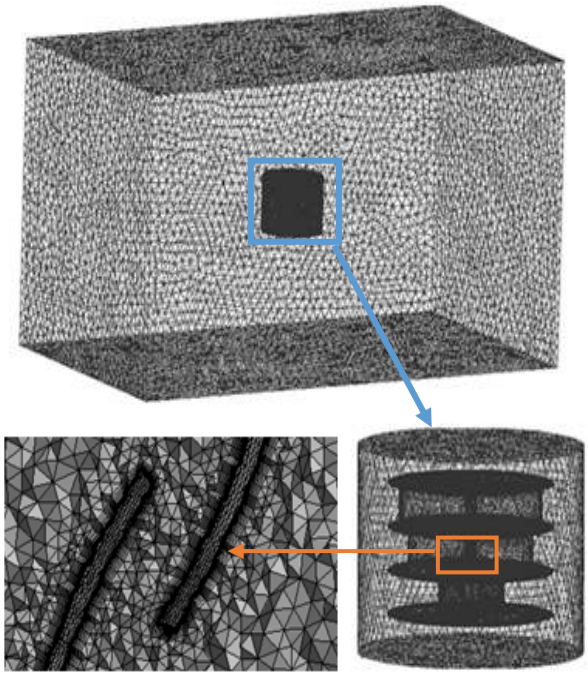

Fig. 8 Mesh generation around the rotor.

Based on the work of a previous study (Alom 2019) the value of time step size for the rotor is chosen 1°/step rotation. The inlet is given as uniform and a constant velocity of V = 6.2 m/s with a 5% turbulence intensity. This value is calculated by:

$$I = \frac{u'}{V}. \quad (7)$$

Where:
v: is the mean velocity (m/s)
u': is the root-mean-square of the turbulent velocity fluctuations calculated from the following equation:

$$u' = \sqrt{\frac{2}{3}k} \quad (m/s) \quad (8)$$

Where k represents the turbulence kinetic energy its value is 0.14415 m^2 /s^2.

Moreover, the pressure outlet is set as Gauge pressure of 0 Pa and sliding wall conditions are utilized at the boundary wall. The CFD codes used the average of the Reynolds Navier Stokes Rans equations for the calculation of turbulent flows. The instantaneous continuity and momentum equations are given by:

$$\frac{\partial \rho}{\partial t} + \frac{\partial}{\partial x_i}(\rho u_i) \quad (9)$$

$$\frac{\partial}{\partial x_i}(\rho u_i) + \frac{\partial}{\partial x_j}(\rho u_i u_j) = -\frac{\partial p}{\partial x_i} + \frac{\partial}{\partial x_i}\left[\mu(\frac{\partial u_i}{\partial x_i} + \frac{\partial u_j}{\partial x_i}) - \frac{2}{3}\delta_{ij}\frac{\partial u_l}{\partial x_l}\right] + \frac{\partial}{\partial x_j}(-\rho\overline{u'_i u'_j}) \quad (10)$$

The Boussinesq hypothesis is used to solve the Reynolds stresses. This hypothesis corresponds to an alignment between the Reynolds stress and the mean strain tensors. Boussinesq equation is expressed as follow:

$$-\rho\overline{u'_i u'_j} = \mu_t(\frac{\partial u_i}{\partial x_j} + \frac{\partial u_j}{\partial x_i}) - \frac{2}{3}(\rho k + \mu_t \frac{\partial u_k}{\partial x_k})\delta_{ij} \quad (11)$$

where μ_t is the turbulent viscosity.

The turbulence is considered to be critical and must be precisely taken into account in the case of CFD simulation. Many different formulations are available for solving turbulent flow problems in the simulation such as standard k-e realizable k-e, RNG k-e, k-ω, SST k-ω, BSL k-ω. In this study, the SST k-ω turbulence model has been utilized (Menter 1994). The SST k- ω model has two partial equations where 'k' refer to turbulence kinetic energy and ω refer to a specific dissipation.

- The kinetic energy of turbulence

$$\frac{\partial k}{\partial t} + \mu_j \frac{\partial k}{\partial x_j} = \frac{\partial}{\partial x_i}\left[(v + \frac{v_t}{\delta_k})\frac{\partial k}{\partial x_j}\right] + G_k - Y_k \quad (12)$$

- Specific dissipation rate

$$\frac{\partial \omega}{\partial t} + \mu_j \frac{\partial \omega}{\partial x_j} = \frac{\partial}{\partial x_i}\left[(v + \frac{v_t}{\delta_\omega}) \frac{\partial \omega}{\partial x_j} \right] + G_\omega - Y_\omega + D_\omega \quad (13)$$

Where:

- v_t = Turbulent eddy viscosity
- G_K = Generation of turbulence kinetic energy owing to mean velocity gradients
- G_ω = Generation of ω
- Y_k and Y_ω = dissipation of k and ω owing to turbulence
- D_ω = the GROSS-diffusion term

3. Results and discussion.

3.1 Numerical simulation validation

In this part, validation is carried out to evaluate the proposed numerical system. The particular results of the simulation of the typical flow around the classical Savonius rotor have been compared to the experimental results obtained by (Sanusi *et al.* 2016). The variation of the power coefficient and torque coefficient, as well as experimental data for different TSR are shown in Figure 9. For both experimental and simulation curves, the highest power coefficient is obtained at TSR = 0.8. For experimental data the C_{Pmax} was 0.24 while for simulation results, the C_{Pmax} was found 0.243. The maximum error value between the experimental and numerical data about 8.8 % for all ranges of TSR. The computational results have a better accord with the experiment test. As a result, it is admissible to perform the numerical method in order to foresee the performance of Savonius rotor.

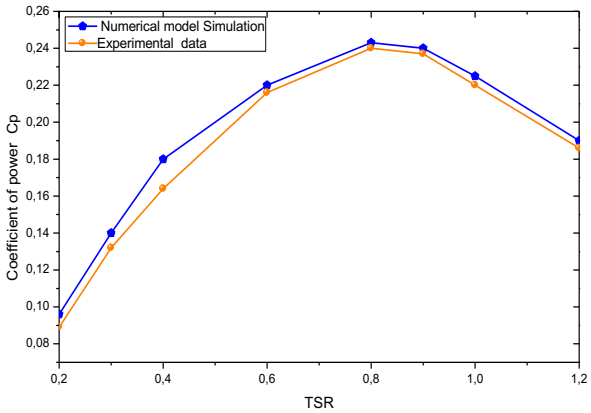

Fig. 9 Experimental (Sanusi et al. 2016) and numerical data of the coefficient of power C_p

Table 2
The maximum coefficient of power C_P and corresponding C_T. (with same RAR of 0. 7)

Rotors	Stage number		
	One	Two	Three
Cpmax	0. 13	0.14	0.19
C_T at Cpmax	0. 153	0.2	0.23

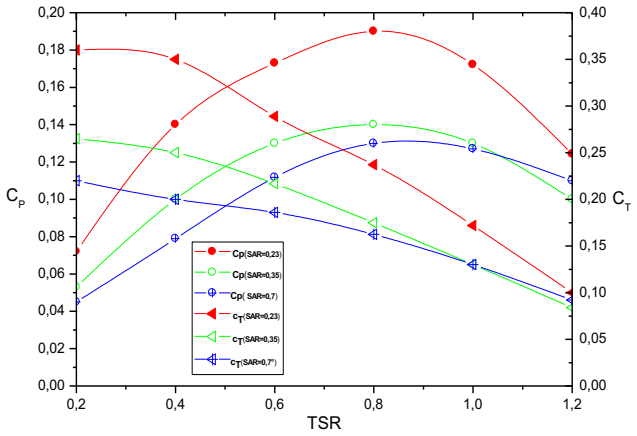

Fig. 10 Power coefficient and Torque coefficient variation.

3.2 Savonius rotors with the similar RAR of 0.7

Figure 10 explains the variations of C_P and C_T with TSR for various stage numbers. In fact, for all the cases the C_T decreases as TSR increases from 0.2 to 1.2, It is observed that the maximum is located at TSR = 0.2. The value of C_T of the three-stage savonius rotor is approximately 27 % higher than that of the two-stage savonius rotor for the range from 0.2 to 0.4 of TSR, while the value of C_T gets closer when TSR > 0.4. The three-stage shows a peak C_P of 0.19 compared to a peak of about 0.14 for the two-stages as illustrated in Fig 10. Thus the C_T value of the two-stage rotor is approximately 15 % higher than that of the one-stage rotor at TSR = 0.2 (and 21% at TSR = 0.4), while the C_T values for one stage is higher than two when TSR > 1. On the other side, the Cp curves of the single and two stage rotors are quite close in TSR range of 0.2 to 0.3 and of 0.9 to 1.2. Indeed, the Cp value of two-stage is higher than that of one stage for TSR lower than 1 as illustrated in Figure 10. However, when TSR > 1, the two stage tends to show a very low decrease compared to other cases. The Cp curve of three-stage is the highest when compared to other stages for all of the range of TSR as illustrated in Figure 10. Additionally, the highest power coefficient (C_{pmax}) happens nearly at TSR = 0.8 for all the rotors.

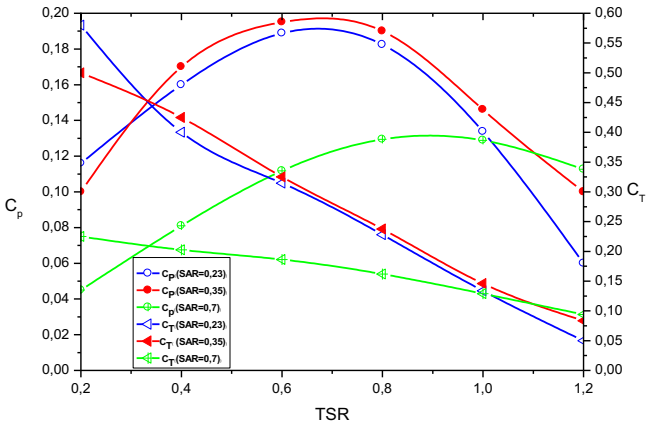

Fig.11 Power coefficient and Torque coefficient variation

The maximum C_P and corresponding C_T increase (for rotors with a similar RAR of 0.7) as a function of the stage numbers as depicted in Table 2. It is more appropriate to use the three stage rotors as they can start automatically due to the uniform static torque coefficient (Kamoji *et al.* 2008).

3.3 Savonius rotors with the similar SAR of 0.7

Figures 11 describes the variations of C_T and C_P with TSR for various stage number (the effect of RAR on the performance). In general, for all the cases the C_T decreases by increasing the TSR. The results reveal that the value of C_T for three -stage is 13.7% higher than the two-stage rotor at 0.2 of the TSR, whereas the C_T values are quite close when TSR varying in the range from 0.4 to 1.2. Moreover, the two-stage rotor shows a C_P peak equal to 0.195, compared to a peak of 0.188 for the three-stage rotors. However, the comparison between one and two-stage rotors proves that the C_T value of the two-stage rotor is higher in the range from 0.2 to 1.1 of TSR, while the values of C_T for two-stage are lower than one-stage when TSR > 1.1.

The Cp curves of the one and two stage rotors are quite approached in the range from 1 to 1.2. The Cp value of two-stage is better than that of one stage for TSR lower than 1.1. In fact, when TSR > 1.1, the two stage rotor tends to show a very low decrease. Further, the two-stage Cp value is the highest in comparison to other stages along with the range 0.3 to 1.2. The maximum power of the coefficient occurs for all rotors between (TSR = 0.6 - 0.8).

In addition, the greatest power coefficient and corresponding C_T increases (for rotors with a similar SAR of 0.7) as the RAR decreases from 2.1 to 1.4. It increases when the RAR increase from 0.7 to 1.4. The Cp of the three and two-stage rotors are quite close in TSR range from 0.3 to 1. For the rotors with a similar SAR of 0.7 (rotors aspect ratio 0.7, 1.4 and 2.1), it has been found in this paper that the two-stage rotor is more efficient than others. (Table 3).

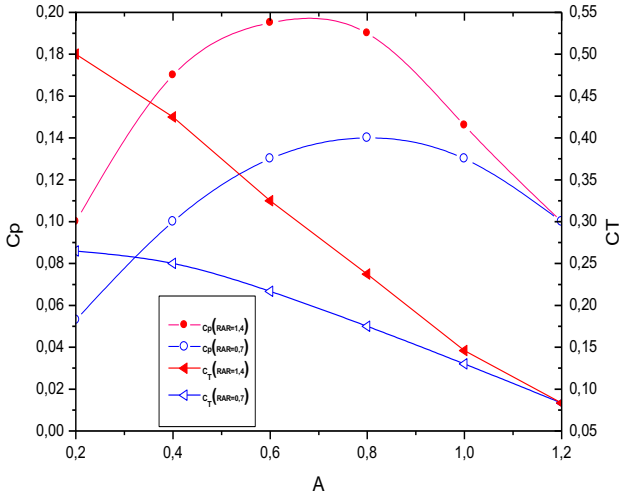

Fig. 12 Power coefficient and Torque coefficient variation for two stage

Table 3
The maximum power and corresponding C_T (with same SAR of 0. 7)

Rotors	Stage number		
	One	Two	Three
Cpmax	0. 13	0.195	0.188
C_T at Cpmax	0. 153	0. 325	0. 314

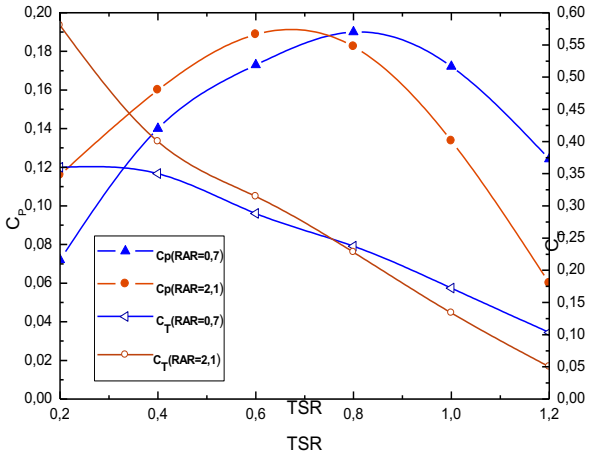

Fig. 13 Power coefficient and Torque coefficient variation for three stage

3. 4 Performance analysis for two-stage elliptical savonius rotors

Every stage of two-stage rotors was placed to one other using a phase shift associated with 90° to one other. Two rotors with a RAR of 0.7 (SAR of 0.35) and RAR of 1.4 (SAR of 0.7) were studied. The Figure 12 shows the comparison in the variation of power coefficient and torque coefficient by varying the TSR for two-stage elliptical rotor wind turbine (RAR of 0.7 and 1.4), the highest power coefficient of the rotor with a RAR of 1.4 is 28.2 % bigger than the savonius rotor with a RAR of 0.7. When TSR > 0.8 the C_p curves associated with two stages rotors are quite close. The coefficient of torque C_T decreases with the increases in the TSR. The highest torque coefficient C_{Tmax} is noticed at a TSR as 0.2, when increasing the TSR the C_T curves associated with two stage rotors are quite close. Two-stage rotor's performance differ after augmenting the SAR and RAR by a factor of 2, which leads to the fact that the SAR has a marginally influence on the performance of the two-stage rotors when the TSR is lower than 1.

3.5 Performance analysis for three-stage elliptical savonius rotors

Every stage of three-stage rotors was placed to one other using a phase shift associated with 60° to one other. Figure 13 shows the comparison in the variation of power coefficient and torque coefficient by varying the TSR three-stage elliptical rotor wind turbine (RAR of 0.7 and

2.1). In the range of TSR between 0.2 and 0.75, the variation of power coefficient shows that the rotor with RAR = 2.1 has a higher performance than that of the rotor with RAR = 0.7, however, after reaching the highest power coefficient, the rotor with RAR = 0.7 tends to show higher performance compared to the rotor with RAR = 2.1.

In the range of TSR between 0.2 and 0.75 the variation of torque coefficient shows that the rotor with RAR = 2.1 has higher C_T values than that of the rotor with RAR = 0.7. When the TSR value increases, the rotor with RAR = 0.7 starts to show higher torque coefficient values.

3.6 *Analysis of pressure and velocity contours*

The streamlines of the flow around the rotor blades at a velocity of 6.2 m/s are shown in Figure 14. When the fluid hits the frontal area of the blades, it generates complex flow in front of the blades. That's why we restrict on the two-dimensional analysis. The total pressure contours on the transverse planes defined in the middle for each stage of the RAT = 0.7 and RAR = 1.4, respectively are shown in Figure 15.

From these results, it has been noted that the higher total pressure is observed on the advancing blade of the elliptical profile (RAR = 1.4) in comparison to the elliptical profiles with (RAR = 0.7) at α = 90°. On the concave side of the returning blade, the total pressure for the elliptical profile (RAR = 1.4) is higher than the elliptical profile (RAR = 0.7). The pressure on the concave side of the blade can contribute to the increase of the positive torque, while the convex side has the possibility to reduce the rotor torque. The depression on the tip of the blade is very important for the elliptical profile (RAR = 1.4) compared to the elliptical profile (RAR = 0.7) at α = 90°, this negative value is due to reverse flow at the tip of the blade. The region of higher pressure on the convex side of the returning elliptical profile for (RAR = 1.4) is lesser as compared to elliptical profile for (RAR = 0.7), and from this result, the torque is higher in the elliptical profile for (RAR = 1.4). For = 0° the magnitude of total pressure near the concave side of the advancing profile is found to be around 2–28 N/m² for elliptical profile (RAR = 1.4), but for the elliptical profile (RAR = 0.7), the range of total pressure is −17 to –25 N/m² at a similar α. As well, it noticed that the concave side of the advancing blade for (RAR = 1.4) shows a higher total pressure compared to the (RAR=0.7).

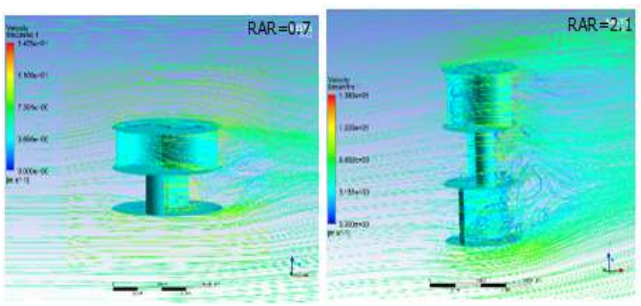

Fig 14. Velocity streamlines

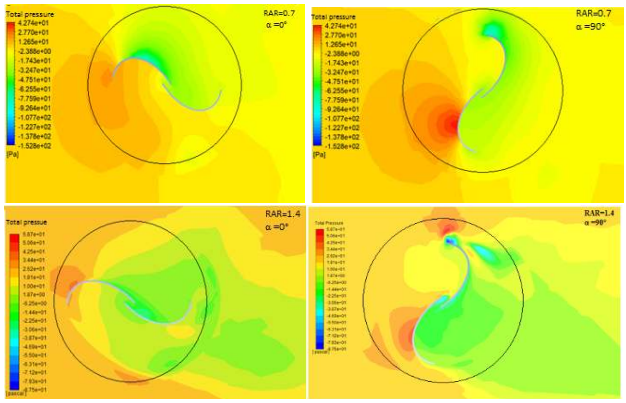

Fig. 15 Contours of Total pressure (Pa) of two stage savonius rotors at TSR = 0.8

Also, the low-pressure zone in the convex side of the returning blade is higher in RAR = 1.4 than the RAR = 0.7. The velocity contours of on the transverse planes defined in the middle for each stage of RAR = 0.7 and RAR = 1.4 respectively are shown in Figure 16. The magnitude of velocity near the surface of the elliptical profile (RAR = 1.4) is approximately in the range of 4-5.75 m/s, whereas in the elliptical profile (RAR = 0.7). The velocity magnitude lies in the range of 3-4.5 m/s. at α =90°. Furthermore, it has been noted that the smaller velocity region on the convex side of the returning elliptical profile (RAR = 1.4) indicates lesser negative drag as compared to the other profile. It is also observed that at the tip of the advancing elliptical blade for (RAR = 1.4), the magnitude of velocity lies in the range of 7-10 m/s, whereas for the other, the velocity magnitude lies in the range of 8-12 m/s at α = 90°. This implies that the chances of flow separation are lower in the case of the elliptical blade for (RAR = 1.4) and this obviously brings an improvement in its performance coefficients. Also, there is a bigger velocity region on the convex side of the advancing elliptical profile (RAR = 1.4) indicating an enhanced positive drag as compared to the elliptical profile (RAR = 0.7). At α = 0°. According to these results, it has been observed the dragging flow on the convex side of the advancing elliptical profile (RAR = 1.4) is more important compared with the elliptical profile (RAR = 0.7).

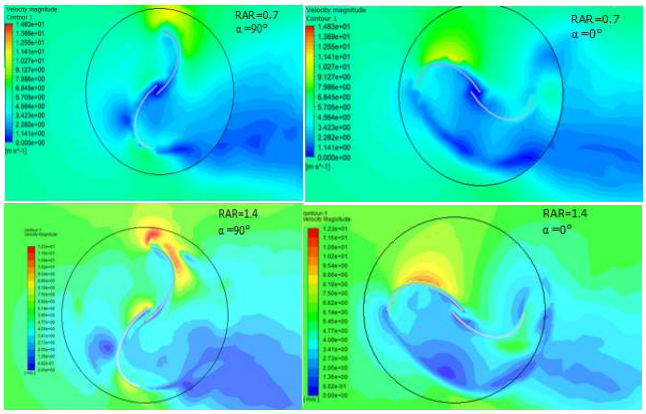

Fig. 16 Contours of the velocity magnitude (m/s) of two stage savonius rotors at TSR = 0.8

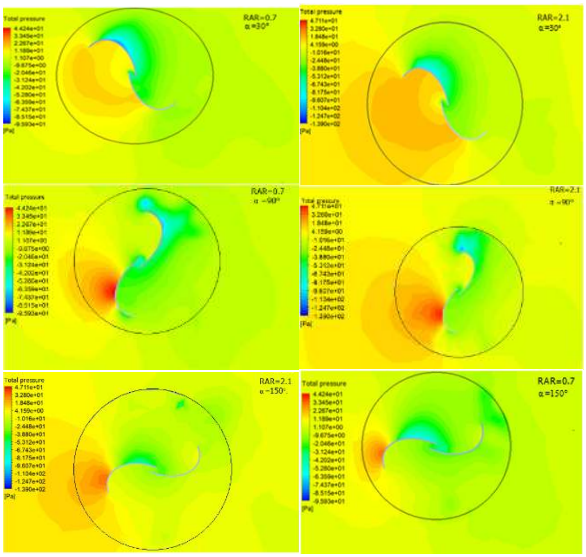

Fig. 17 contours of Total pressure (Pa) of three stage savonius rotors at TSR = 0.8

The total pressure contours on the transverse planes defined in the middle for each stage of the RAT = 0.7 and RAR = 2.1 respectively are shown in Figure 17. For α = 90°, the magnitude of the total pressure near the concave side of the advancing blade is around 2-12 Pa for the elliptical profile (RAR = 0.7), however, for the elliptical profile (RAR = 2.1) the total pressure range is -10 to 4 Pa at a similar α, whereas, on the convex side of the returning blade, the total pressure for the elliptical profile (RAR = 2.1) is higher than the elliptical profile (RAR = 0.7). For α = 30°, the low-pressure area behind the advancing blade that forms the recirculation is higher in the elliptical profile (RAR = 2.1) than in the elliptical profile (RAR = 0.7). In addition, the higher pressure area on the convex side of the returning blade for (RAR = 0.7) is less than the other, and therefore the resulting torque is higher in the elliptical profile for (RAR = 0.7).

At the rotor angle of 150° ,on the basis of these results, it was found that the concave side of the advancing blade for (RAR = 0.7) shows a higher total pressure compared to the (RAR = 2.1). Also, the pressure distribution around the convex side of returning blade for a (RAR = 2.1) is almost similar to that of a (RAR = 0.7).

4. Conclusion

In this numerical investigation, the effect of stage number on the efficiency of a savonius wind turbine is studied by developing a 3 D numerical simulation using the SST k-ω turbulence model. The wind speed is 6.2 m/s and the flow is considered as three-dimensional, incompressible and turbulent. The results of the simulation around the conventional blade of savonius wind turbine reveal good accordance with the previous works. The Comparison between one, two and three stage rotors with the similar RAR which equals 0.7 indicates that the maximum of the coefficient of power increases as a function of the number of stages. For rotors with a similar SAR of 0.7 (rotors aspect ratio 0.7, 1.4 and 2.1), it has been found that the two-stage rotor is more efficient than others

Nomenclature

Cp	power coefficient $Cp = 2\ P/\ HDRV^3$	dimensionless
P	Power	W
R	Radius of rotor	m
H	Rotor height	m
D	Rotor diameter	m
V	Wind velocity,	m/s
C_T	coefficient of torque $C_T = 4\ T\ /RV^2D^2H$	dimensionless
T	Torque.	N.m
Ω	Rotor angular speed	rad/s
λ	Tip speed ratio $\lambda = \Omega D/2V$	dimensionless
AR	aspect ratio H/D	dimensionless
K	Turbulent kinetic energy	J.kg-1
ω	Specific dissipation rate	1/s
Re	Reynolds number, $Re = \rho VD/\upsilon$	dimensionless
ρ	Density of air	kg/m^3
RAR	Rotor aspect ratio	dimensionless
SAR	Rotor aspect ratio	dimensionless

References

Akwa, J. V., da Silva Júnior, G. A., & Petry, A. P. (2012). Discussion on the verification of the overlap ratio influence on performance coefficients of a Savonius wind rotor using computational fluid dynamics. *Renewable energy*, 38(1), 141-149.

Aldos, T. K. (1984). Savonius rotor using swinging blades as an augmentation system. *Wind Engineering*, 214-220.

Aldoss, T. K., & Najjar, Y. S. (1985). Further development of the swinging-blade Savonius rotor. *Wind Engineering*, 165-170.

Alom, N., Kolaparthi, S. C., Gadde, S. C., & Saha, U. K. (2016). Aerodynamic design optimization of elliptical-bladed Savonius-style wind turbine by numerical simulations. ASME 2016 35th International Conference on Ocean, Offshore and Arctic Engineering.

Alom, N., & Saha, U. K. (2017). Arriving at the optimum overlap ratio for an elliptical-bladed Savonius rotor. ASME Turbo Expo 2017: Turbomachinery Technical Conference and Exposition.

Alom, N., & Saha, U. K. (2018). Performance evaluation of vent-augmented elliptical-bladed savonius rotors by numerical simulation and wind tunnel experiments. *Energy*, 152, 277-290.

Alom, N., and Saha, U.K. (2019). Drag and lift characteristics of a novel elliptical-bladed Savonius rotor with vent augmenters. *Journal of Solar Energy Engineering* 141.

Altan, B. D., & Atılgan, M. (2010). The use of a curtain design to increase the performance level of a Savonius wind rotors. *Renewable Energy*, 35(4), 821-829.

Bach, G. von. (1931). Untersuchungen über Savonius-rotoren und verwandte strömungsmaschinen. Forschung auf dem Gebiet des Ingenieurwesens A, 2(6), 218-231.

Banerjee, A., Roy, S., Mukherjee, P., & Saha, U. K. (2014). Unsteady flow analysis around an elliptic-bladed Savonius-style wind turbine. ASME 2014 Gas Turbine India Conference.

Benesh, A. H. (1988). Wind turbine system using a vertical axis savonius-type rotor. Google Patents.

Blackwell, B. F., Feltz, L. V., & Sheldahl, R. E. (1977). Wind tunnel performance data for two-and three-bucket Savonius rotors. Sandia Laboratories Springfield, VA, USA.

Chen, J., Chen, L., Nie, L., Xu, H., Mo, Y., & Wang, C. (2016). Experimental study of two-stage Savonius rotors with different gap ratios and phase shift angles. Journal of *Renewable and Sustainable Energy*, 8(6), 063302.

ElCheikh, A., Elkhoury, M., Kiwata, T., & Kono, T. (2018). Performance analysis of a small-scale orthopter-type vertical axis wind turbine. *Journal of Wind Engineering and Industrial Aerodynamics*, 180, 19-33.

Frikha, S., Driss, Z., Ayadi, E., Masmoudi, Z., & Abid, M. S. (2016). Numerical and experimental characterization of multi-stage Savonius rotors. *Energy*, 114, 382-404.

Golecha, K., Eldho, T. I., & Prabhu, S. V. (2011). Influence of the deflector plate on the performance of modified Savonius water turbine. *Applied Energy,* 88(9), 3207-3217.

Grinspan, A. S., Kumar, P. S., Mahanta, P., Saha, U. K., Rao, D. R., & Bhanu, G. V. (2001). Design, development & testing of Savonius wind turbine rotor with twisted blades. Proceedings 28th National Conference on Fluid Mechanics and Fluid Power, Dec, 13-15.

Hayashi, T., Li, Y., & Hara, Y. (2005). Wind tunnel tests on a different phase three-stage Savonius rotor. JSME *International Journal Series B Fluids and Thermal Engineering*, 48(1), 9-16.

Johannes, S. S. (1929). Rotor adapted to be driven by wind or flowing water. Google Patents.

Kacprzak, K., Liskiewicz, G., & Sobczak, K. (2013). Numerical investigation of conventional and modified Savonius wind turbines. *Renewable energy*, 60, 578-585.

Kamoji, M. A., Kedare, S. B., & Prabhu, S. V. (2008). Experimental investigations on single stage, two stage and three stage conventional Savonius rotor. *International Journal of Energy Research*, 32(10), 877-895.

Kamoji, M. A., Kedare, S. B., & Prabhu, S. V. (2009). Experimental investigations on single stage modified Savonius rotor. *Applied Energy*, 86(7-8), 1064-1073.

Mahmoud, N. H., El-Haroun, A. A., Wahba, E., & Nasef, M. H. (2012). An experimental study on improvement of Savonius rotor performance. *Alexandria Engineering Journal*, 51(1), 19-25.

Mendoza, V., Katsidoniotaki, E., and Bernhoff, H. (2020). Numerical Study of a Novel Concept for Manufacturing Savonius Turbines with Twisted Blades. *Energies* 13, 1874.

Menet, J.-L. (2004). A double-step Savonius rotor for local production of electricity : A design study. *Renewable energy*, 29(11), 1843-1862.

Menter, F. R. (1994). Two-equation eddy-viscosity turbulence models for engineering applications. *AIAA journal*, 32(8), 1598-1605.

Mojola, O. O. (1985). On the aerodynamic design of the Savonius windmill rotor. *Journal of Wind Engineering and Industrial Aerodynamics*, 21(2), 223-231.

Nugroho, A.D., Tjahjana, D.D.D.P., and Kristiawan, B. (2020). Slotted blade effect on Savonius wind rotor performance. In AIP Conference Proceedings, (AIP Publishing LLC), p. 030102.

Ogawa, T., Yoshida, H., & Yokota, Y. (1989). Development of rotational speed control systems for a Savonius-type wind turbine. *J. Fluids Eng*. 111(1), 53-58

Roy, S., & Saha, U. K. (2013a). Investigations on the effect of aspect ratio into the performance of Savonius rotors. ASME 2013 Gas Turbine India Conference.

Roy, S., & Saha, U. K. (2013b). Review of experimental investigations into the design, performance and optimization of the Savonius rotor. Proceedings of the Institution of Mechanical Engineers, Part A: Journal of Power and Energy, 227(4), 528-542.

Roy, S., & Saha, U. K. (2015). Wind tunnel experiments of a newly developed two-bladed Savonius-style wind turbine. *Applied Energy*, 137, 117-125.

Saha, U. K., & Rajkumar, M. J. (2006). On the performance analysis of Savonius rotor with twisted blades. *Renewable energy*, 31(11), 1776-1788.

Saha, U. K., Thotla, S., & Maity, D. (2008). Optimum design configuration of Savonius rotor through wind tunnel experiments. *Journal of Wind Engineering and Industrial Aerodynamics*, 96(8-9), 1359-1375.

Sanusi, A., Soeparman, S., Wahyudi, S., & Yuliati, L. (2016). Experimental study of combined blade savonius wind turbine. *International Journal of Renewable Energy Research (IJRER)*, 6(2), 614-619.

Savonius, S. J. (1931). The S-rotor and its applications. Mechanical engineering, 53(5), 333-338.

Scheaua, F.D. (2020). Comparative Numerical Analysis on Vertical Wind Turbine Rotor Pattern of Bach and Benesh Type. *Energies* 13, 2311.

Zemamou, M. abdelghani toumi, khalid mrigua, yahya lahlou, et mohammed aggour,(2020). A novel blade design for savonius wind turbine based on polynomial bezier curves for aerodynamic performance enhancement. *Int. J. Green Energy*, doi: 10.1080/15435075.2020.1779077.

Zemamou, M., Toumi, A., Mrigua, K., & Aggour, M. (2019.). Modified Design of Savonius Wind Turbine Blade for Performance Improvement. *International Journal of Innovative Technology and Exploring Engineering,* 9(1),1432-1437.